Tgfbr2 disruption in postnatal smooth muscle impairs aortic wall homeostasis

Wei Li,[1,2] Qingle Li,[1,2] Yang Jiao,[1] Lingfeng Qin,[1] Rahmat Ali,[1] Jing Zhou,[1] Jacopo Ferruzzi,[3] Richard W. Kim,[1] Arnar Geirsson,[1,4] Harry C. Dietz,[5] Stefan Offermanns,[6] Jay D. Humphrey,[3] and George Tellides[1,4]

[1]Department of Surgery and Interdepartmental Program in Vascular Biology and Therapeutics, Yale University School of Medicine, New Haven, Connecticut, USA. [2]Department of Vascular Surgery, Peking University People's Hospital, Beijing, People's Republic of China. [3]Department of Biomedical Engineering and Interdepartmental Program in Vascular Biology and Therapeutics, Yale University, New Haven, Connecticut, USA. [4]Veterans Affairs Connecticut Healthcare System, West Haven, Connecticut, USA. [5]Department of Pediatrics, Johns Hopkins University School of Medicine, Baltimore, Maryland, USA. [6]Department of Pharmacology, Max-Planck-Institute for Heart and Lung Research, Bad Nauheim, Germany.

TGF-β is essential for vascular development; however, excess TGF-β signaling promotes thoracic aortic aneurysm and dissection in multiple disorders, including Marfan syndrome. Since the pathology of TGF-β overactivity manifests primarily within the arterial media, it is widely assumed that suppression of TGF-β signaling in vascular smooth muscle cells will ameliorate aortic disease. We tested this hypothesis by conditional inactivation of *Tgfbr2*, which encodes the TGF-β type II receptor, in smooth muscle cells of postweanling mice. Surprisingly, the thoracic aorta rapidly thickened, dilated, and dissected in these animals. *Tgfbr2* disruption predictably decreased canonical Smad signaling, but unexpectedly increased MAPK signaling. Type II receptor–independent effects of TGF-β and pathological responses by nonrecombined smooth muscle cells were excluded by serologic neutralization. Aortic disease was caused by a perturbed contractile apparatus in medial cells and growth factor production by adventitial cells, both of which resulted in maladaptive paracrine interactions between the vessel wall compartments. Treatment with rapamycin restored a quiescent smooth muscle phenotype and prevented dissection. *Tgfbr2* disruption in smooth muscle cells also accelerated aneurysm growth in a murine model of Marfan syndrome. Our data indicate that basal TGF-β signaling in smooth muscle promotes postnatal aortic wall homeostasis and impedes disease progression.

Introduction

TGF-β, comprising 3 isoforms and acting via a heteromeric complex of TGF-β type I and II receptors (TβRI and TβRII, respectively), has pleiotropic effects throughout development (1). Animal models allow these effects to be studied longitudinally. Germline deletions in mice of *Tgfbr1* or *Tgfbr2*, which encode TβRI and TβRII, cause midgestational death due to vascular defects of the yolk sac (2, 3). Moreover, selective deletion of *Tgfbr1* and *Tgfbr2* in smooth muscle recapitulates the vascular deformities and embryonic lethality of global deletion (4). Even gene deletion restricted to specific smooth muscle lineages leads to vascular abnormalities and perinatal death (5–7). Although germline genetic modifications have provided valuable insight into TGF-β signaling in vascular morphogenesis, they are not suitable for studying mechanisms of vascular homeostasis or disease progression that occur postnatally. In humans, Loeys-Dietz syndrome, which is caused by heterozygous mutations in *TGFBR1* or *TGFBR2*, often presents in young adults with complications of aortic dissection or aneurysm rupture (8). Even though the mutant receptors cannot transduce TGF-β–mediated signals (9, 10), tissues obtained at surgery paradoxically suggest enhanced TGF-β signaling in vivo (8, 11). Excessive TGF-β activity is also observed in the media of aortic aneurysms from patients with Marfan syndrome caused by mutations of *FBN1* (encoding fibrillin-1) as well as in patients with a phenotype similar to that seen in Loeys-Dietz and Marfan disorders, which is caused by mutations in *TGFB2* or *SMAD3* (11–13). Similarly, upregulation of

TGF-β signaling is found in nonsyndromic aortic disease caused by mutations in *MYH11* (encoding smooth muscle myosin heavy chain [SMMHC]) and *ACTA2* (encoding SMA) as well as undefined etiologies (14, 15). Increased TGF-β activity has been hypothesized as resulting from impaired sequestration of latent TGF-β complexes in the extracellular matrix by aberrant fibrillin-1 in Marfan syndrome (16) and from greater production of TGF-β in the overlapping phenotype due to *TGFB2* mutations (12, 13). Increased TGF-β signaling associated with aortic disease is inferred from nuclear accumulation of phosphorylated Smad2 (p-Smad2), a canonical signaling mediator of TGF-β, and increased expression of typical TGF-β–inducible molecules in clinical specimens. Similar findings of TGF-β overactivity are evident in mouse models of Marfan syndrome caused by *Fbn1* deletion or mutation (16–18). Treatment of these animals with TGF-β antagonists prevents phenotypic manifestations of Marfan syndrome (16, 17). Based on these promising experimental results, clinical trials of losartan, an angiotensin receptor blocker that also antagonizes TGF-β signaling, have been initiated in patients with Marfan syndrome (19). Yet recent studies uncovered a more complex relationship in which noncanonical TGF-β signaling also promotes aneurysm formation in mouse models of Marfan syndrome, primarily through MAPK cascades, including p38 and ERK1/2 pathways (18, 20). The mechanisms by which these perturbations in signaling cause aortic disease remain poorly understood, however. In both syndromic and nonsyndromic aortic diseases, it is generally believed that pathological effects of hyperactive TGF-β signaling are intrinsic to vascular smooth muscle and that suppression of TGF-β responses in this cell type will prevent dissection and aneurysm formation. Here, we directly test this hypothesis using a genetically defined animal model.
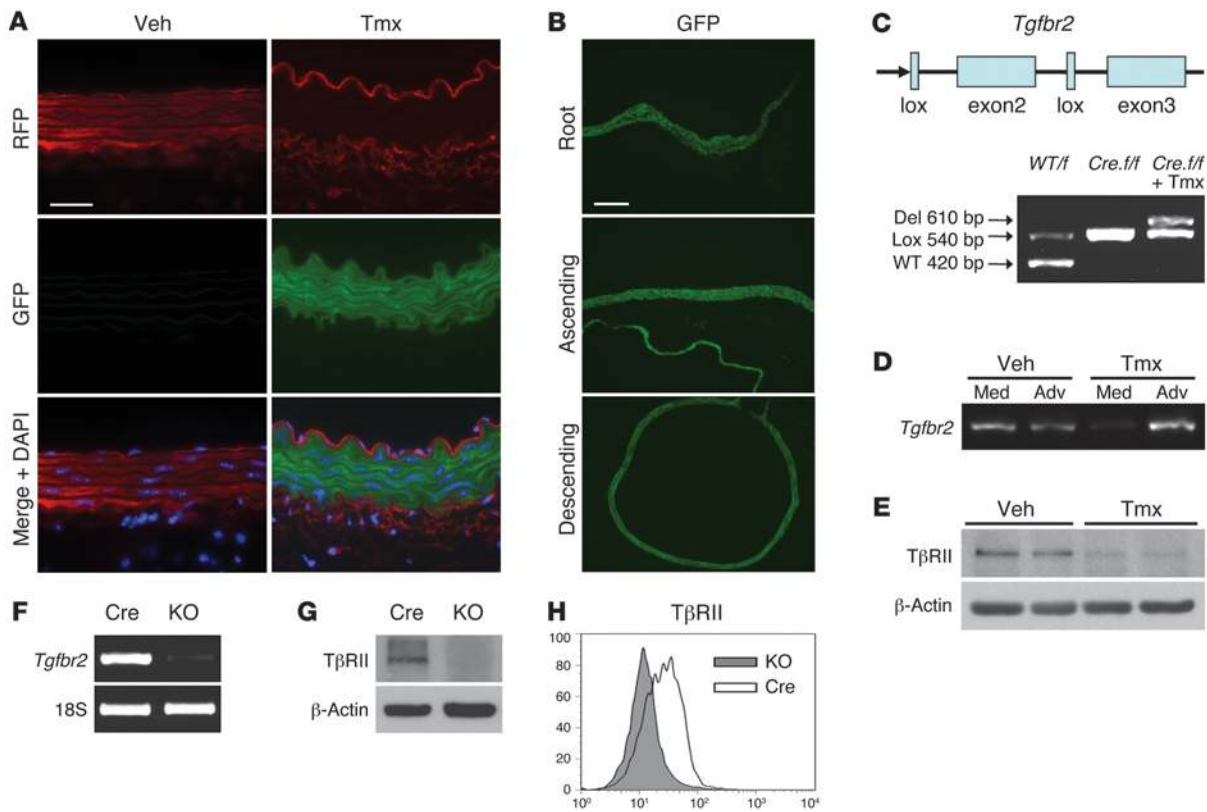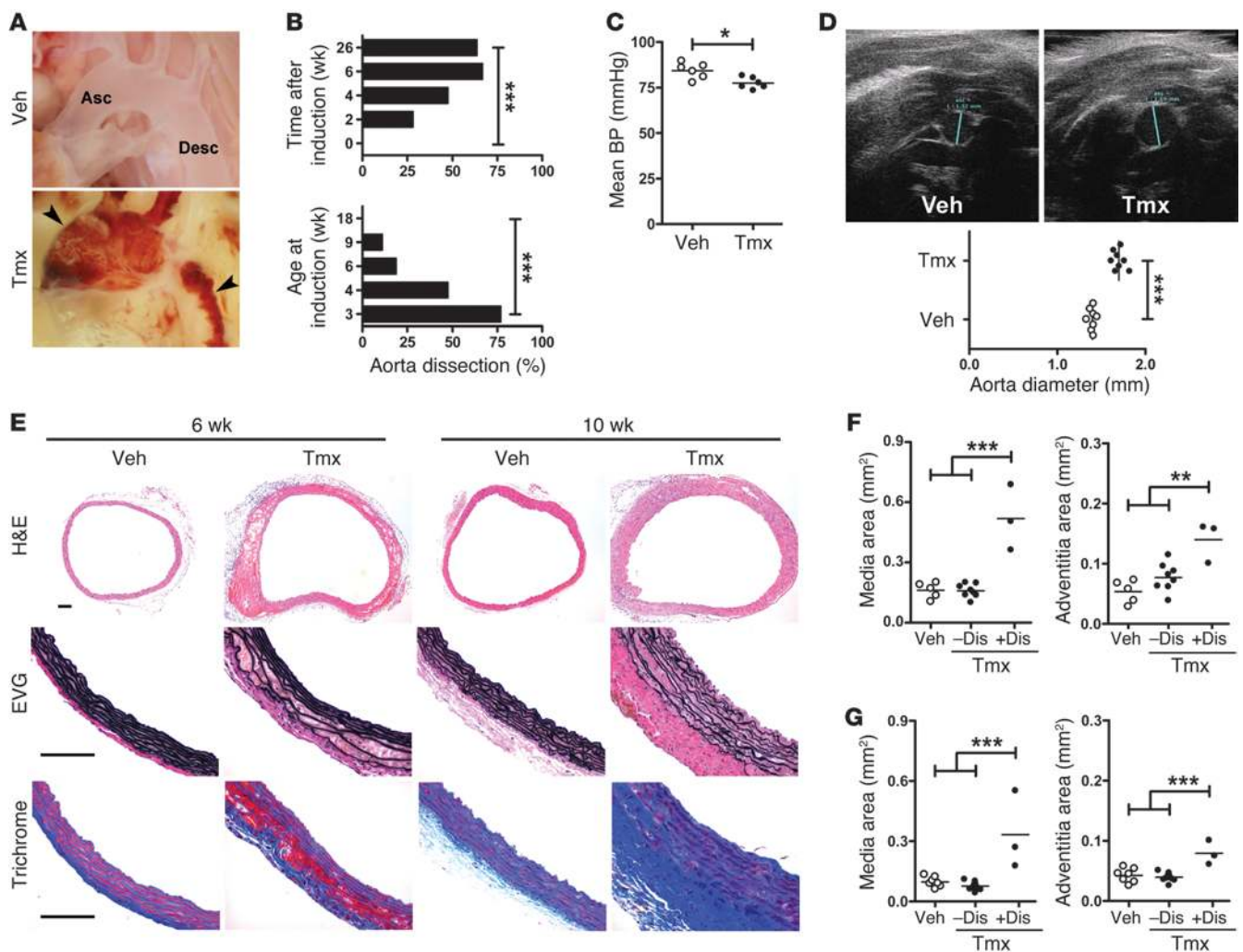
Figure 1
Conditional disruption of *Tgfbr2* in smooth muscle of postnatal mice. (**A**) Selective expression of GFP and loss of RFP in medial, but not intimal or adventitial, cells of *mT/mG.Myh11-CreER*[T2]*.Tgfbr2*[f/f] mice after vehicle (Veh) or tamoxifen (Tmx) treatment; nuclei stained with DAPI. Scale bar: 30 μm. (**B**) Diffuse Cre-mediated GFP expression in the aortic root, ascending aorta (and adjacent pulmonary artery), and descending aorta. Scale bar: 150 μm. (**C**) Scheme of *Tgfbr2* floxed allele and PCR for 420 bp WT, 540 bp floxed (Lox), and 610 bp Cre-deleted (Del) bands in abdominal aortas of *Tgfbr2*[WT/f] and *Myh11-CreER*[T2]*.Tgfbr2*[f/f] mice without and with tamoxifen treatment. (**D**) *Tgfbr2* detection in media (Med) and adventitia (Adv) from thoracic aortas of *Myh11-CreER*[T2]*.Tgfbr2*[f/f] mice treated with vehicle or tamoxifen and (**E**) TβRII expression in the isolated medial tissue. (**F**) PCR for *Tgfbr2 exon2* mRNA expression and (**G**) immunoblotting and (**H**) flow cytometric analysis for TβRII extracellular domain expression in GFP[+] SMCs cultured from thoracic aortas of *mT/mG.Myh11-CreER*[T2] (Cre) and *mT/mG.Myh11-CreER*[T2]*.Tgfbr2*[f/f] (KO) mice after tamoxifen induction.

Results

Conditional disruption of Tgfbr2 in smooth muscle of postnatal mice. We investigated whether TGF-β is required for continued integrity of the developed vasculature by inactivating TβRII in postweanling mice; this receptor is essential for ligand binding and transphosphorylation of TβRI (1). To circumvent embryonic lethality, mice homozygous for *Tgfbr2* in which exon2 was flanked with *loxP* sites (21) were bred with mice expressing Cre recombinase fused with a modified estrogen receptor–binding domain (ER[T2]) under control of a smooth muscle–specific *Myh11* promoter (22). Dual transgene expression allows inducible Cre activity and deletion of floxed DNA segments by injection of a synthetic estrogen, tamoxifen. Specificity and efficiency of gene modification were assessed by intercrossing to *mT/mG* double-fluorescent reporter mice that ubiquitously express the product of a floxed gene for membrane-targeted Tomato, a variant red fluorescent protein (RFP), except where deleted by Cre to express membrane-targeted GFP, which marks recombined cells (23). After tamoxifen treatment of *mT/mG.Myh11-CreER*[T2]*.Tgfbr2*[f/f] mice, SMCs selectively and robustly expressed GFP in all segments of the aorta (Figure 1, A and B). Recombination of floxed *Tgfbr2* alleles was confirmed, although

unmodified gene sequence was still detected in aortic tissue consisting of several vascular layers and cell types (Figure 1C). Separation of the aortic wall into inner muscular and outer fibrous layers demonstrated tamoxifen-mediated deletion of *Tgfbr2* within the media (Figure 1D). Correspondingly, TβRII expression was markedly decreased in medial tissue (which still contained endothelium after removing the adventitia) following tamoxifen induction (Figure 1E). GFP[+] SMCs were propagated after explant growth and flow cytometric sorting to exclude any nonrecombined or contaminating cells, such as fibroblasts (Supplemental Figure 1; supplemental material available online with this article; doi:10.1172/JCI69942DS1). Expression of mRNA for *Tgfbr2 exon2* or the encoded TβRII extracellular domain was not detected in KO cells (Figure 1, F–H). These data show successful disruption of *Tgfbr2* in the aortic media of postnatal mice and the ability to select bona fide SMCs for in vitro experiments.

Tgfbr2 disruption rapidly results in disease of the thoracic aorta. We examined the phenotype of *Myh11-CreER*[T2]*.Tgfbr2*[f/f] mice after tamoxifen treatment. There was rapid development of aortic dissection, revealed by mural hematoma on gross examination, in a subset of KO animals that progressively increased in incidence

Figure 2
Tgfbr2 disruption in smooth muscle results in aortic thickening, dilatation, and dissection. (**A**) Gross appearance of ascending (Asc) and descending (Desc) thoracic aorta (arrows mark mural hematomas) in 8-week-old *Myh11-CreER^T2^.Tgfbr2^f/f^* mice treated with vehicle or tamoxifen for 5 days starting at 4 weeks of age. (**B**) Aortic dissection rates at various times after tamoxifen treatment of 4-week-old mice (0/28 after 0 weeks, 11/39 after 2 weeks, 19/40 after 4 weeks, 4/6 after 6 weeks, and 7/11 weeks after 26 weeks) or at 4 weeks after induction starting at different ages (10/13 at 3 weeks, 19/40 at 4 weeks, 3/16 at 6 weeks, 1/9 at 9 weeks, and 0/7 at 18 weeks). ***$P < 0.001$, χ^2 test. (**C**) Aortic blood pressure of 6-week-old mice treated with vehicle or tamoxifen at 4 weeks of age; $n = 6$. *$P < 0.05$, t test. (**D**) Representative ultrasound images and ascending aorta diameters (blue lines) of 6-week-old mice treated with vehicle or tamoxifen at 4 weeks of age; $n = 8$. ***$P < 0.001$, t test. (**E**) H&E, EVG, and trichrome stains of the ascending aorta from 6- and 10-week-old mice treated with vehicle or tamoxifen at 4 weeks of age demonstrating progressive elastin fragmentation, elastic lamella widening, adventitial fibrosis, and mural thickening. Scale bars: 100 μm. (**F**) Medial and adventitial areas of ascending aortas with or without dissection (Dis) in 8-week-old mice treated with vehicle or tamoxifen at 4 weeks of age and (**G**) similar analysis of descending thoracic aortas; $n = 3–12$. **$P < 0.01$, ***$P < 0.001$, 1-way ANOVA.

with time depending on the age at induction (Figure 2, A and B). Younger animals, with a higher incidence of aortic dissection, also had more extensive disease (Supplemental Figure 2A). Aortic rupture or unexpected deaths were not observed from 2 to 26 weeks after tamoxifen treatment at 4 weeks of age; thus, this induction protocol was used for most of the subsequent experiments. Hemorrhage of the aortic wall usually began in the proximal ascending or proximal descending segments, and occasionally, intimal flaps and false lumens were identified (Supplemental Figure 2, A and B). The dissections often extended into arch branches, but the abdominal aorta was rarely involved (2 of 180 mutants). Injury of the vessel wall was not due to hypertension, as central blood pressure was

modestly reduced in KO mice (Figure 2C). Consistent dilatation of the ascending aorta was noted by 6 weeks of age irrespective of dissection occurrence (Figure 2D). In the presence of dissection, mural thickening characterized by elastin fragmentation, elastic lamella widening, and adventitial fibrosis evolved between 6 and 10 weeks (Figure 2E). Leukocytes accumulated in the underlying adventitia in association with erythrocyte extravasation into the media; acellular medial foci developed by 10 weeks, and medial degeneration progressed circumferentially by 30 weeks (Supplemental Figure 2, C–F). In the absence of dissection, the aortic wall in KO mice displayed few morphological abnormalities with rare infiltrating leukocytes up to 10 weeks of age, but medial degenera-
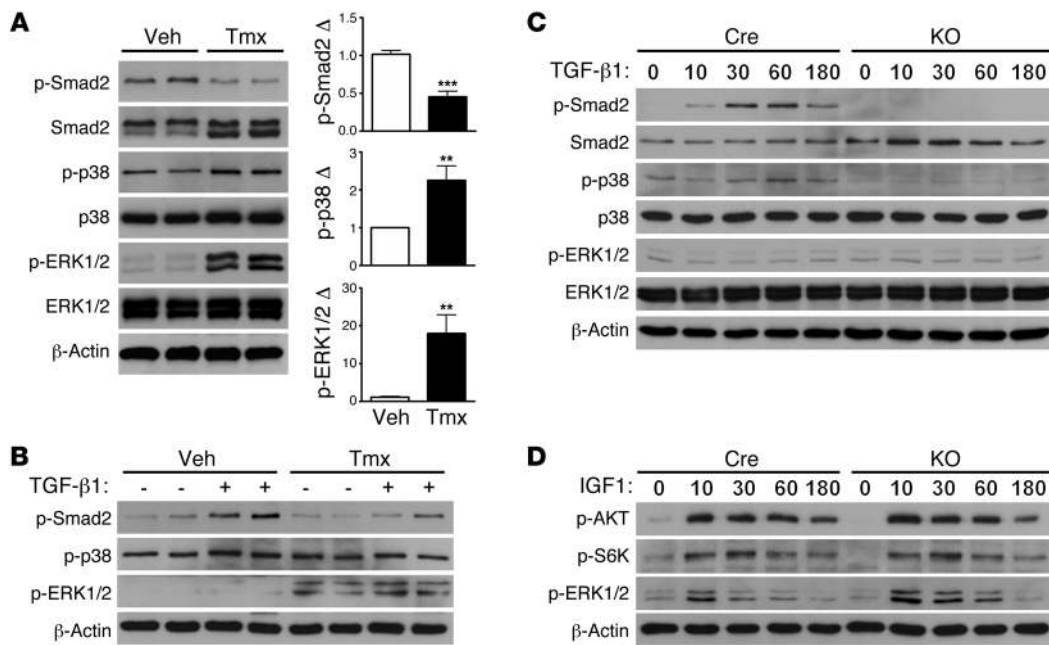
Figure 3
TβRII inactivation reduces canonical Smad signaling, but leads to increased MAPK signaling. (**A**) Immunoblotting for phosphorylated and total Smad2, p38, and ERK1/2 in nondissected thoracic aortas from 6-week-old *Myh11-CreER^T2.Tgfbr2^f/f* mice treated with vehicle or tamoxifen at 4 weeks of age; band densities were normalized to corresponding β-actin bands and expressed as a fraction of a control value, *n* = 6. **P* < 0.01; ***P* < 0.001, *t* test. (**B**) Expression of signaling mediators in thoracic aorta segments cultured in serum-free medium for 3 hours and then treated with TGF-β1 at 10 ng/ml or vehicle for 1 hour. (**C**) Expression of signaling mediators in GFP+ SMCs cultured from thoracic aortas of tamoxifen-induced *mT/mG.Myh11-CreER^T2* (Cre) and *mT/mG.Myh11-CreER^T2.Tgfbr2^f/f* (KO) mice, serum-deprived for 24 hours, and then treated with TGF-β1 at 1 ng/ml or (**D**) IGF1 at 100 ng/ml for 0–180 minutes.

tion and adventitial thickening were apparent by 30 weeks even without evidence of mural ecchymosis (Supplemental Figure 3). The histological changes in dissected aortas manifested as significant medial and adventitial expansion within 4 weeks of induction (Figure 2, F and G). Adventitial fibrosis was associated with increased transcript expression for extracellular matrix molecules and TGF-β isoforms in the aortic wall of KO mice (Supplemental Figure 4). Global inhibition of TGF-β signaling by serologic neutralization did not alter the rate of aortic dissection, but diminished adventitial collagen accumulation, prevented adventitial thickening, and resulted in several sudden deaths from transmural aortic bleeding (Supplemental Figure 5). Aortic disease was not observed 2 to 4 weeks after heterozygous loss of *Tgfbr2* (*n* = 8). Additionally, there was no vascular pathology in tamoxifen-treated *mT/mG.Myh11-CreER^T2* mice lacking *Tgfbr2^f/f* (*n* = 12) or in *Tgfbr2^f/f* mice lacking *Myh11-CreER^T2* (*n* = 6), which excluded an artifact of the induction strategy.

Loss of TβRII responsiveness diminishes Smad2 signaling. To determine signaling changes after *Tgfbr2* disruption that may drive aortic disease, we evaluated canonical and noncanonical TGF-β signaling via Smad and MAPK pathways, respectively (18, 20). Nondissected thoracic aortas from 6-week-old mice were analyzed to minimize confounding effects from bleeding, inflammation, and remodeling. Adherent adventitia and endothelium were not removed due to technical difficulties and the possibility of triggering injury-related signaling. Immunoblotting demonstrated decreased p-Smad2 (despite greater Smad2 expression), but increased p-p38 and p-ERK1/2 in KO aorta (Figure

3A). Parallel signaling changes of lesser magnitude were seen after heterozygous *Tgfbr2* disruption (Supplemental Figure 6A). Decreased Smad2 phosphorylation and increased ERK1/2 phosphorylation were localized to the media of KO aorta (Supplemental Figure 6B). MAPK activation due to signaling in rare nonrecombined SMCs or by TβRII-independent effects of TGF-β in KO aorta was excluded using neutralizing antibody (Supplemental Figure 7). The divergence in Smad and MAPK signaling was further investigated in vitro by TGF-β treatment of cultured aortas or SMCs. TGF-β1–mediated activation of Smad2 and p38 was reduced in KO aorta (TβRII-expressing fibroblasts, endothelial cells, or nonrecombined SMCs may have contributed to residual signaling), although ERK1/2 responses were not detected even in treated aortic tissue from noninduced mice (Figure 3B). A caveat is that baseline (untreated) levels of p-p38 and p-ERK1/2 were greater in cultured KO aortas in keeping with their prior in vivo activation following tamoxifen induction. TβRII inactivation also abolished TGF-β1–mediated Smad2 and p38 phosphorylation in isolated GFP+ SMCs, whereas ERK1/2 activation was not apparent in treated control or KO cells at the times and doses tested (Figure 3C). Similar signaling responses were seen after treatment with TGF-β2 and TGF-β3 (Supplemental Figure 8). We confirmed that signaling, including that of ERK1/2, was intact in cultured SMCs in response to another trophic mediator, IGF1 (Figure 3D). Our data show that stimulation of Smad2 in aortic media by TGF-β under homeostatic conditions is mediated through TβRII expressed on SMCs, while p38 and ERK1/2 are activated in the absence of TβRII responsiveness in the same cells.
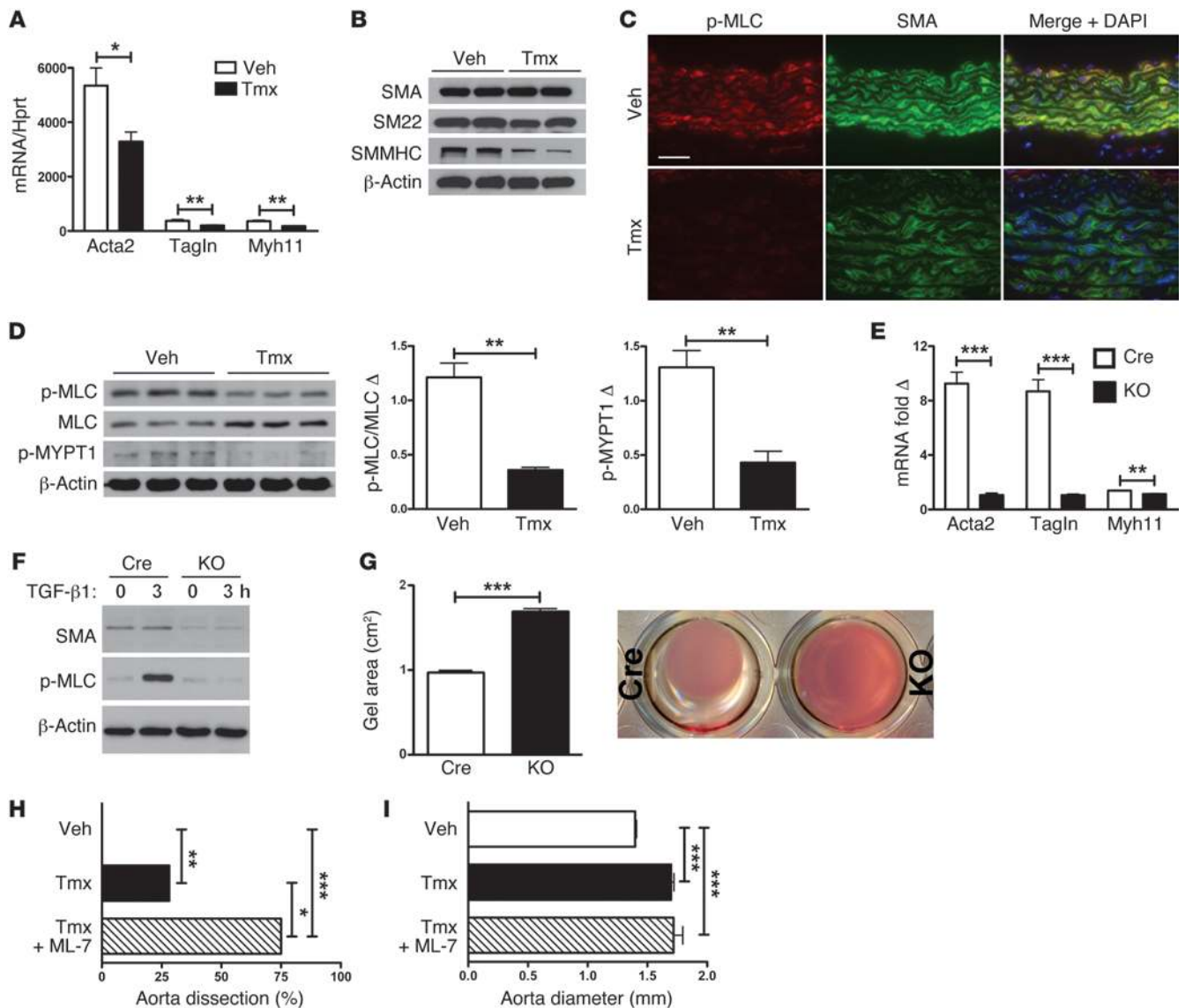
Figure 4
Loss of TGF-β signaling impairs the contractile apparatus of vascular smooth muscle. (**A**) Quantitative PCR for Acta2, Tagln, Myh11 and (**B**) immunoblots for their encoded products SMA, SM22, and SMMHC in thoracic aortas of 6-week-old *Myh11-CreER^T2.Tgfbr2^f/f* mice treated with vehicle or tamoxifen at 4 weeks; *n* = 6. *P < 0.05; **P < 0.01, *t* test. (**C**) Immunofluorescence analysis for p-MLC and SMA at 30 weeks. Scale bar: 30 μm. (**D**) Expression of total and p-MLC and p-myosin phosphatase target subunit-1 (MYPT1) at 6 weeks; *n* = 3. **P < 0.01, *t* test. (**E**) Transcript expression (fold-change treated/untreated) in GFP+ SMCs cultured from tamoxifen-induced *mT/mG.Myh11-CreER^T2* (Cre) or *mT/mG.Myh11- CreER^T2.Tgfbr2^f/f* (KO) mice, serum-deprived for 24 hours, and treated or not with TGF-β1 at 1 ng/ml for 6 hours; *n* = 3. **P < 0.01; ***P < 0.001, *t* test. (**F**) Cultured KO SMCs show reduced expression of SMA before treatment and lack of MLC activation after treatment with TGF-β1 at 1 ng/ml for 3 hours. (**G**) Collagen gel disc contraction by embedded SMCs after 72 hours in 10% serum-supplemented medium; *n* = 3. ***P < 0.001, *t* test. (**H**) Aortic dissection rate in mice treated or not with the MLC kinase inhibitor, ML-7 at 73 μg/d s.c. constant infusion from 4–6 weeks of age; *n* = 0/28 (vehicle), 11/39 (tamoxifen), and 6/8 (tamoxifen+ML-7). *P < 0.05; **P < 0.01; ***P < 0.001, χ² test. (**I**) Ascending aorta diameter in these animals at 6 weeks; *n* = 5–8. ***P < 0.001, 1-way ANOVA.

Loss of TGF-β signaling impairs the contractile apparatus of vascular smooth muscle. To determine mechanisms of aortic disease after TβRII inactivation, we assessed the expression of smooth muscle contractile molecules, since many contain TGF-β control elements in their promoter regions and their inherited abnormalities may predispose to aortic disease (24, 25). Although we found decreased transcript expression for Acta2, Tagln, and Myh11 in aorta from 6-week-old KO mice (Figure 4A), there was variable or no differ-

ence in their protein expression at this early time point (Figure 4B and Supplemental Figure 9A). Decreased immunolabeling for SMA was apparent by 10 and at 30 weeks of age (Figure 4C and Supplemental Figure 9B). Given that diminished blood pressure, aortic dilatation, and a subset of aortic dissection by 6 weeks preceded consistent changes in contractile protein expression, we also assessed the phosphorylation of myosin light chain (MLC) — a key regulator of myosin-actin interactions and a known target
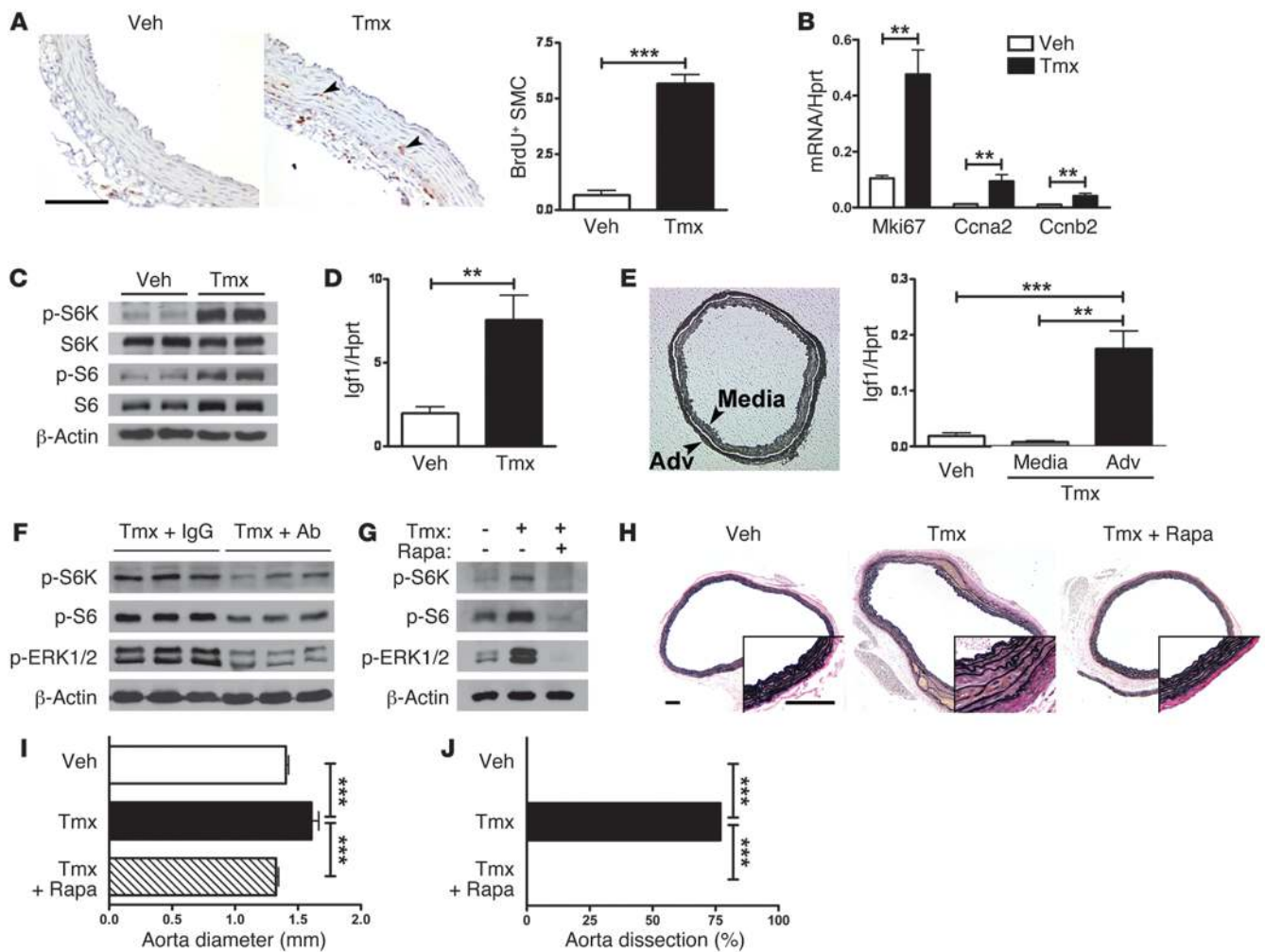
Figure 5
Loss of TGF-β signaling induces vascular cell proliferative responses. (**A**) Immunohistochemistry for BrdU incorporation (brown color, arrows) with hematoxylin counter-staining of nuclei in thoracic aortas of 6-week-old *Myh11-CreER^T2^.Tgfbr2^f/f^* mice treated with vehicle or tamoxifen at 4 weeks of age. Scale bar: 100 μm, BrdU⁺ medial cells per cross-section, n = 3, ***P < 0.001, t test. (**B**) Quantitative RT-PCR for Mki67, Ccna2, and Ccnb2; n = 6, **P < 0.01, t test and (**C**) immunoblotting for total and p-S6K and S6 in thoracic aortas at 6 weeks. (**D**) Igf1 transcript expression in full-thickness thoracic aortas at 6 weeks; n = 6, P < 0.01, t test or in (**E**) adventitia (Adv) separated from media (arrows) by laser capture microdissection at 10 weeks; n = 3, **P < 0.01, ***P < 0.001, 1-way ANOVA. (**F**) Expression of activated S6K, S6, and ERK1/2 in thoracic aortas of KO mice treated with isotype-matched IgG or IGF1 antibody (Ab) at 125 μg/d i.p., q.o.d. from 4–6 weeks or (**G**) treated with rapamycin (Rapa) at 2 mg/kg/d i.p., q.d. from 3–7 weeks. (**H**) EVG stains with higher magnification of vessel wall shown in insets. Scale bar: 100 μm and (**I**) diameter of ascending aortas in 7-week-old mice induced with vehicle or tamoxifen at 3 weeks of age and treated or not with rapamycin as above; n = 10–11, ***P < 0.001, 1-way ANOVA. (**J**) Aortic dissection rate in these animals; n = 0/11 (vehicle), 10/13 (tamoxifen), and 0/11 (tamoxifen+rapamycin), ***P < 0.001, χ² test.

of TGF-β signaling (26, 27). Strikingly, p-MLC was significantly decreased (despite increased MLC expression) early after TβRII knockdown, and it persisted long-term (Figure 4, C and D, and Supplemental Figure 9B). We further investigated the regulation of MLC phosphorylation that is governed by kinases and phosphatases. Decreased phosphorylation of myosin phosphatase target subunit-1 after TβRII inactivation (Figure 4D) was consistent with deactivation of this inhibitory component and consequently increased myosin phosphatase activity and dephosphorylation of MLC (26). Similar findings regarding structural and regulatory contractile molecules were also seen in cultured cells. TGF-β induced *Acta2*, *Tagln*, and *Myh11* mRNA expression in control, but not KO, SMCs (Figure 4E). KO cells expressed lower basal levels of

contractile proteins, and the robust phosphorylation of MLC in response to TGF-β treatment was prevented by TβRII inactivation (Figure 4F). Diminished expression of SMA was associated with an irregular rounded appearance of KO cells in culture compared with spindle-shaped control cells (Supplemental Figure 10, A–C). Decreased contractility of KO SMCs was demonstrated in a collagen gel system (Figure 4G). A pathogenetic role for impaired MLC activity was confirmed in vivo by treating KO mice with an MLC kinase inhibitor that significantly increased the rate of aortic dissection, but not the degree of aortic dilatation (Figure 4, H and I). These data are concordant with the clinical phenotype of aortic dissection with little to no enlargement of the aorta seen in families with mutations of *MYLK* encoding MLC kinase (28).
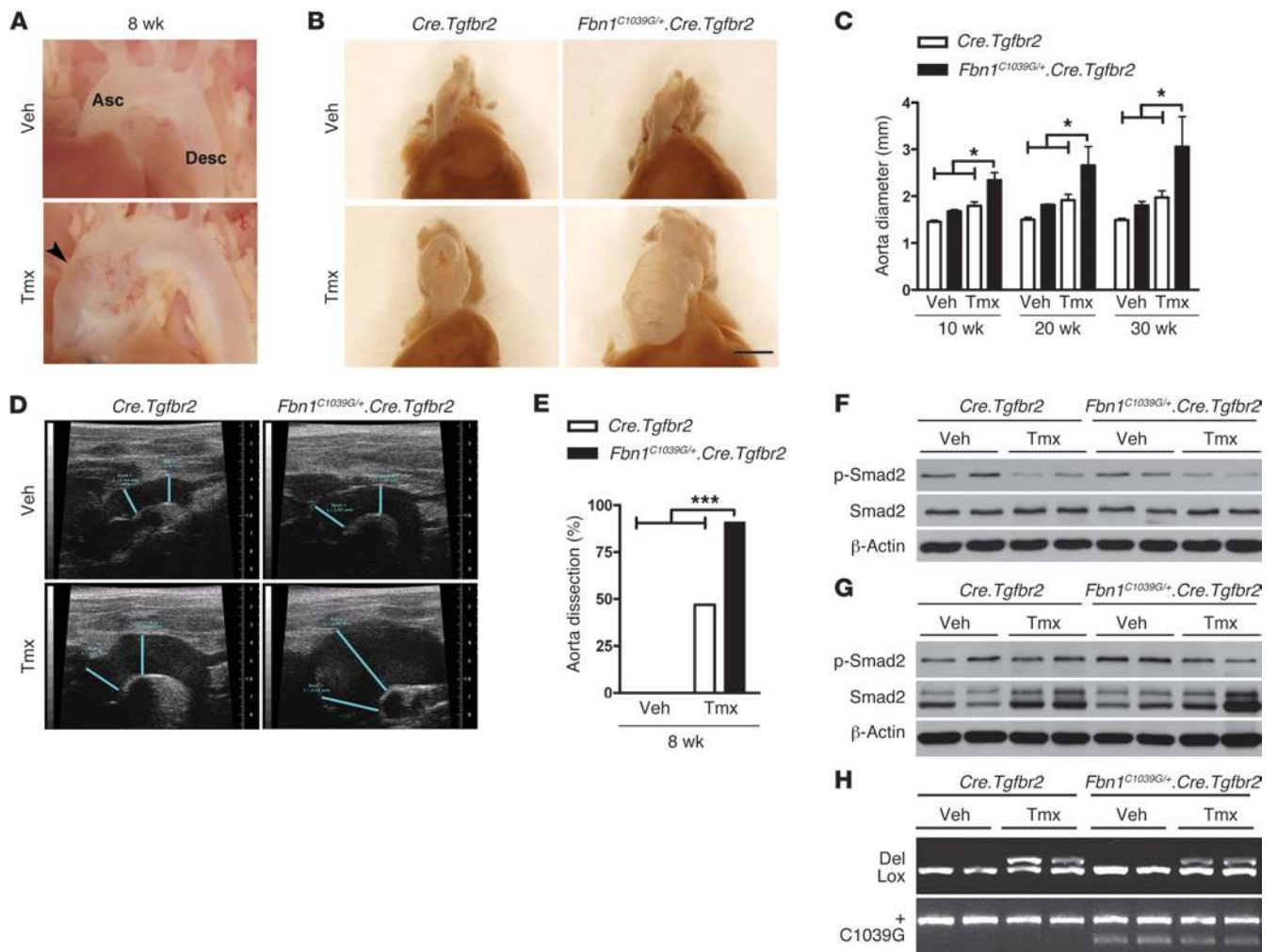
Figure 6
TβRII inactivation exacerbates mutant fibrillin-1–induced aortic disease. (**A**) Gross appearance of thoracic aorta (arrow marks dissected aneurysm) in 8-week-old *Fbn1^C1039G/+*.Myh11- CreER^T2.Tgfbr2^f/f* mice treated with vehicle or tamoxifen for 5 days starting at 4 weeks of age. (**B**) Thoracic aortas of 30-week-old *Myh11-CreER^T2.Tgfbr2^f/f* (*Cre.Tgfbr2*) and *Fbn1^C1039G/+*.Myh11- CreER^T2.Tgfbr2^f/f* littermates treated with vehicle or tamoxifen. (**C**) Ascending aorta diameters by serial ultrasound imaging at 10, 20, and 30 weeks; *n* = 3–4. *$P < 0.05$, 1-way ANOVA. (**D**) Representative images of aortic root and ascending aorta diameters (blue lines) at 30 weeks. (**E**) Aortic dissection rates at 8 weeks; *n* = 0/20 (WT), 0/15 (mutant *Fbn1*), 15/32 (*Tgfbr2* KO), and 20/22 (compound mutant). ***$P < 0.001$, χ^2 test. (**F**) Immunoblotting for phosphorylated and total Smad2 in nondissected aortas at 5 weeks and (**G**) at 30 weeks. (**H**) PCR for deleted (del) vs. floxed (lox) *Tgfbr2* and WT (+) vs. mutant (C1039G) *Fbn1* in abdominal aorta specimens.

Loss of TGF-β signaling elicits vascular cell proliferation. We searched for additional pathogenetic effects of TβRII inactivation, since genetic disruption of contractile molecule expression or activity in mice does not result in overt aortic dissection or aneurysm phenotypes (28–30). We assessed for excessive SMC proliferation, as TGF-β has well-described growth regulatory effects (1) and medial hyperplasia is associated with certain aortic diseases (31–33). BrdU incorporation revealed increased cell division in all layers of the aortic wall after loss of TGF-β signaling in smooth muscle, particularly in the outer media and adventitia (Figure 5A). Cultured KO SMCs also displayed increased BrdU incorporation in response to serum stimulation (Supplemental Figure 10D). Transcript analysis of KO aortas confirmed increased expression of proliferation markers and cell-cycle regulators (Figure 5B). Immunoblotting

demonstrated greater phosphorylation of mTOR effectors characteristic of mitogenic responses (Figure 5C). However, activation of the mTOR pathway, like that of ERK1/2, was unlikely a direct effect of TβRII knockdown, as exogenous TGF-β did not suppress mTOR signaling of SMCs in vitro, but actually led to phosphorylation of mTOR targets in delayed fashion (Supplemental Figure 11A). To screen for secondary mediators of mTOR activation after *Tgfbr2* disruption, we performed a genome-wide analysis by DNA microarray hybridization of KO versus control aorta. Of 120 transcripts with altered expression, including numerous proliferation markers and cell cycle regulators (Supplemental Table 1; microarray data from this table have also been deposited in the Gene Expression Omnibus; GSE36778), we focused on the induction of IGF1 — a key growth factor related to aneurysm formation

in inherited abnormalities of smooth muscle contractile proteins (33). Increased production of IGF1 after TβRII inactivation was confirmed by quantitative techniques (Figure 5D). Using laser capture microdissection of aortic wall layers, more than 95% of IGF1 transcription was localized to the adventitia of KO aorta (Figure 5E). A paracrine role for adventitial-derived IGF1 in smooth muscle mitogenic signaling was verified by its serologic neutralization, which reduced mTOR and ERK1/2 activation (Figure 5F). The role of SMC proliferation was further investigated using a pharmacological inhibitor of mTOR signaling. Rapamycin administered at 2 mg/kg/d, a validated therapeutic dose in other models of arterial disease characterized by SMC hyperplasia (34, 35), resulted in whole-blood trough levels of 27.3 ± 5.0 ng/ml (n = 6). This treatment strategy inhibited mTOR and ERK1/2 signaling of KO aorta in vivo (Figure 5G). In vitro, rapamycin at 10–100 ng/ml abolished IGF1-mediated mTOR, but not ERK1/2 signaling, in cultured KO SMCs (Supplemental Figure 11B). Rapamycin did not normalize the expression of p-Smad2 after tamoxifen induction (Supplemental Figure 12A). Remarkably, however, rapamycin treatment completely prevented degeneration, dilatation, and dissection of the aorta even under the more stringent conditions of early disruption of *Tgfbr2* at 3 weeks of age (Figure 5, H–J). Prevention of aortic disease was associated with diminished expression of proliferation markers and cell-cycle regulators as well as decreased SMC hyperplasia and medial expansion, although IGF1 production and the expression or activity of contractile molecules was not affected (Supplemental Figure 12, B–E). Rapamycin administration also did not modulate the number of sparse perivascular leukocytes or the absence of medial infiltrates (Supplemental Figure 12F). These data suggest that SMC proliferation represents a pathological response to loss of TGF-β signaling and is not merely a marker for another growth factor–mediated pathogenic process, e.g., SMC dedifferentiation, or for an inflammatory effect.

TβRII inactivation exacerbates mutant fibrillin-1–mediated aortic disease. Finally, we interbred *Fbn1^C1039G/+* and *Myh11-CreER^T2.Tgfbr2^f/f* mice to test the hypothesis that aortic disease attributable to mutant fibrillin-1 is prevented by inhibition of TGF-β signaling in smooth muscle (17, 20). Remarkably, there were more severe pathological changes of the aorta in compound mutant mice than in those with mutant fibrillin-1 alone (Figure 6, A and B, and Supplemental Figure 13). Serial ultrasound measurements showed faster and larger ascending aorta aneurysm formation in compound mutant mice, which approached twice the diameter seen in controls by 30 weeks (Figure 6C). Similarly, the aortic root was 1.5 to 1.9 times larger than that in control or single mutant mice at 30 weeks (P < 0.01, 1-way ANOVA, n = 3–4). Unlike in *Fbn1^C1039G/+* mice, the ascending aorta was consistently larger than the aortic root after *Tgfbr2* disruption (Figure 6D). Aortic dissection manifested as early as 5 weeks and was almost uniformly present by 8 weeks in compound mutant mice (Figure 6E). Immunoblotting of nondissected specimens confirmed diminished Smad2 activation after TβRII inactivation on WT and mutant *Fbn1* backgrounds (0.38- and 0.24-fold normalized expression levels, respectively) at 5 weeks (Figure 6F). These differences were largely lost by 30 weeks, and increased phosphorylation of Smad2 in aortas of *Fbn1^C1039G/+* mice (1.7-fold normalized expression levels) was evident at this late time point (Figure 6G). Despite more severe pathological changes, the abnormalities in signaling, contractile molecules, and proliferation were not greater in compound mutants at either early or late time points (Supplemental Figures 14 and 15), although the

degree of *Tgfbr2^f/f* recombination was not uniform between the aortas from WT versus mutant *Fbn1* backgrounds (Figure 6H). The differences in dissection occurrence, in sites of maximal aneurysmal dilatation, and the lack of correlation between phenotype severity and inferred pathogenic events suggest different mechanisms of aortic disease resulting from TβRII inactivation than for fibrillin-1 mutation.

Discussion

We conclude (a) that basal TGF-β signaling in smooth muscle is required to preserve structural integrity and maintain quiescent interactions between medial and adventitial compartments of the thoracic aorta following normal embryonic development and (b) inactivation of these TβRII-dependent responses in SMCs exacerbates aortic disease in a model of Marfan syndrome. Although there are similarities in the medial degeneration and aortic dissection of our animals with human disease (11–15), we do not suggest that our strategy of inducible *Tgfbr2* deletion in smooth muscle of postnatal animals models Loeys-Dietz syndrome attributable to heterozygous *TGFBR2* point mutations in the germline of patients. Mice with analogous *Tgfbr2* point mutations will be the optimal experimental system to model this disease. The observed phenotype in our animals depends strongly on the age at which *Tgfbr2* is disrupted. Younger mice had a greater incidence of aortic dissection, suggesting a sensitivity of growing arteries to basal TGF-β signaling, not unlike prenatally developing vessels (5–7). Greater cellular proliferation and extracellular matrix production distinguished both developing and growing aortas from mature ones. We speculate that cell division transiently alters SMC contractile apparatus and cell-matrix interactions, which may predispose the vessel wall to complications of dissection and dilatation. However, our studies in older mice terminated at 4 weeks after induction were limited, and we cannot exclude delayed onset of disease with longer observation periods. The adult aorta with comparatively fewer requirements in cellular and extracellular matrix turnover to maintain wall integrity may not manifest pathology due to underlying genetic predispositions unless subjected to further vascular injury or increased hemodynamic loading.

Our conclusions are contingent upon ablation of TGF-β signaling in SMCs after *Tgfbr2* disruption. A previous report verified no binding of radiolabeled TGF-β1 to TβRI after Cre-mediated deletion of *Tgfbr2* in fibroblasts (21). We found that both TGF-β–mediated Smad2 activation and Smad-independent p38 activation (36) were eliminated after TβRII inactivation in cultured SMCs. We did not find immediate activation of ERK1/2 by TGF-β in murine SMCs, known to be delayed and to depend on protein synthesis in certain cell types (37) and TβRII in cell types with rapid activation (38). Our experiments with isolated KO cells in vitro and neutralizing antibodies in vivo do not support TβRII-independent signaling by TGF-β in postnatal SMCs, as recently described for embryonic cranial neural crest cells (39). The p38 and ERK1/2 activation following TβRII inactivation in vivo is likely an indirect effect that results from stress-related and/or growth factor–mediated responses, since exogenous TGF-β does not directly affect MAPK signaling of KO cells in vitro. We show that increased ERK1/2 signaling in KO aorta is at least partly due to adventitia-derived IGF1. It has been previously documented in *Fbn1*-null mice that stress-related MAPK activation can lead to promiscuous Smad2 activation in SMCs independently of TGF-β signaling (18) and this crosstalk may also explain apparent normalization of
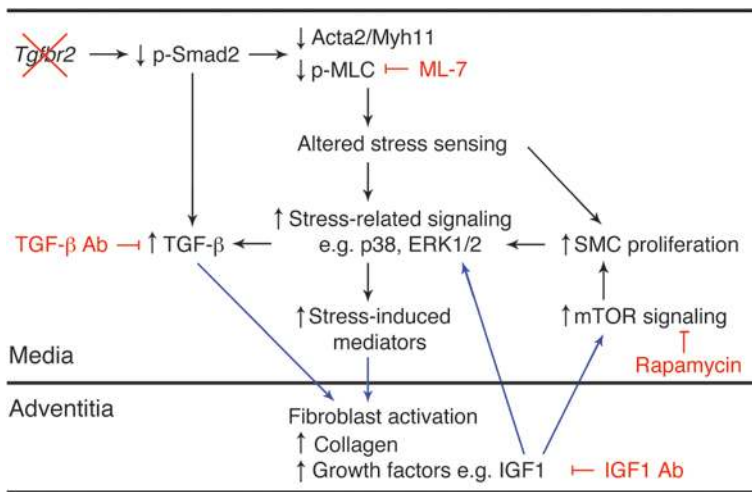
Figure 7
Schematic representation of the essential role for TGF-β in postnatal aortic wall homeostasis. *Tgfbr2* disruption in SMCs leads to loss of basal Smad signaling, decreased expression and activity of contractile molecules (via MYPT1 for effects on MLC), and altered stress-related signaling (e.g., of the MAPKs p38 and ERK1/2) likely due to altered hemodynamic stress sensing through cytoskeleton/integrin/extracellular matrix links. Increased TGF-β may be a compensatory response to diminished p-Smad2 signaling and/or a direct effect of altered mechanical stress. Additional stress-induced mediators may include reactive oxygen species and cytokines as found in other models of arterial remodeling (45). Paracrine effects (blue arrows) by secreted soluble molecules from medial cells activate adventitial fibroblasts, leading to increased collagen accumulation, growth factor production (e.g., IGF1), and fibroblast proliferation. Adventitial thickening may represent a reparative "injury" response and contribute to mural integrity. Reciprocal paracrine effects (blue arrows) on medial cells by adventitial-derived mediators contribute to increased mTOR signaling and SMC proliferation that exacerbate stress-related responses. The outcome of these transcompartmental interactions is maladaptive cellular and extracellular matrix remodeling; disease manifests as aortic dilatation and/or dissection. We tested this hypothesis with several pharmacological and blocking antibody reagents (red font), all of which modulated the phenotype. Additional studies are required to validate the concept of altered stress sensing after *Tgfbr2* disruption as recently reported for *Acta2*-deficient mice in which loss of SMA leads to increased focal adhesion kinase signaling resulting in MAPK activation and autonomous SMC proliferation (30). Possible further interactions with endothelial cells and circulating/resident leukocytes were not considered.

p-Smad2 expression at 30 weeks of age following *Tgfbr2* disruption besides an increased number of TβRII-responsive adventitial cells constituting the degenerated vessel wall at this late time point.

We describe several mechanisms that link loss of TGF-β signaling in smooth muscle to aortic dissection and dilatation. Contractile dysfunction is thought to underlie aortic aneurysm and dissection due to *MYH11* and *ACTA2* mutations in humans (25), and dedifferentiation of aortic SMCs harboring *TGFBR2* missense mutations from clinical specimens has been described (10). In mice, *Myh11* mutation and *Acta2* deletion cause a milder phenotype characterized by abnormalities in vascular contractility without overt aortic disease; additional vascular injury in these strains unmasks a gain in proliferative function of SMCs (29, 30). Although contractile protein expression gradually and modestly declines in our *Tgfbr2* KO aortas, the early and robust loss of MLC phosphorylation correlates better with the rapid onset of vascular disease following TβRII inactivation. This conclusion is supported by clinical findings showing that loss-of-function muta-

tions in *MYLK* encoding MLC kinase associate with aortic dissection (28). Thus, modulating MLC activity, either directly or through its kinase and phosphatase regulatory enzymes, may have utility in aortic disease treatment. However, smooth muscle–specific knockdown of *Mylk* in mice causes medial degeneration without mural dissection (28) — suggesting cooperative effects of diminished MLC activity with additional disease precipitants in our model. Hyperplastic medial remodeling was first described in thoracic aortic aneurysms as a compensatory response to increased tensile stress or as a driver of vessel growth and expansion (31). More recently, hyperplastic vasculomyopathy has been reported as a pathological manifestation resulting from *ACTA2* mutations (32). Moreover, patients with loss-of-function mutations in *TSC2*, an inhibitor of mTOR, have vascular disease, including aortic aneurysms, and SMCs from mice with heterozygous loss of *Tsc2* are characterized by increased mTOR signaling and proliferation (34). We found that rapamycin prevents aortic dissection and dilatation in addition to suppressing smooth muscle mitogenesis. The precise benefits of rapamycin in this setting require further definition, but may relate to effects on SMC cytoskeleton organization besides its antiproliferative properties (40). Inhibition of mTOR signaling in vascular cells represents what we believe is a novel therapeutic approach to preventing aortic disease, although additional work is required to exclude an immunosuppressive effect as the relevant mechanism (41, 42). However, a concern against the use of cytostatic agents is that fibroblast hyperplasia and adventitial thickening contribute to vessel wall integrity and may prevent fatal transmural rupture. Nonetheless, a gain in proliferative function may be a cause as well as a consequence of SMC dedifferentiation. Similarly to recent findings by the Milewicz group in *Myh11*-mutant and *Acta2*-deficient mice (29, 30), we hypothesize that altered SMC mechanosensing may link the contractile dysfunction, MAPK activation, and medial hyperplasia that occur after *Tgfbr2* disruption (Figure 7).

Our results highlight the paracrine interactions between vascular compartments and the need to consider whole tissues in context (43). In our model, the media is the primary site of signaling alterations that are reflected in the aortic tissue immunoblots at 6 weeks of age. Within 2 weeks of TβRII inactivation, contractile apparatus perturbations are evident, with consistent changes in blood pressure and blood vessel size and partial occurrence of medial dissection. The adventitia, of normal appearance at this initial disease stage, undergoes reactive changes over several weeks (in the presence of medial dissection) to months (in the absence of medial dissection); these changes are associated with growth factor production, cellular hyperplasia, and collagen deposition. The majority of the adventitial cells appear to be fibroblasts with relatively few SMA-expressing myofibroblasts (44). The reparative responses are ineffective, and the media progressively degenerates over 30 weeks. We have identified IGF1 as one mediator of the trans-compartmental interaction. In a similar system of *Tgfbr2* disruption in stromal fibroblasts, increased production of hepatocyte growth factor caused neoplasia of adjacent epithelia (21). It is likely that several other

intermediaries contribute to bidirectional signaling between the vascular layers, e.g., reactive oxygen species and cytokines (45, 46). The importance of the adventitia in vascular disease is increasingly being recognized, and a greater understanding of inflammation, fibroblast activation, and resident precursor cell niches in this compartment have contributed to an integrated view of vessel layer functions in vascular remodeling (47, 48).

Our finding of a protective role for basal TGF-β signaling in *Fbn1*[C1039G/+] mice suggests that the beneficial effects of systemic TGF-β neutralization previously seen in the same model may accrue from effects on cell types other than SMCs (17). It is possible that partial inhibition of excess signaling in the media (due to limited antibody penetration into this avascular compartment) is not equivalent to complete ablation of resting TGF-β activity in SMCs. An important difference is that the vascular phenotype is restricted to the aortic root and proximal ascending aorta in mouse models of Marfan syndrome (17, 20), whereas disease manifestation, signaling changes, and expression differences are present throughout the thoracic aorta after *Tgfbr2* disruption, albeit more pronounced in the ascending aorta. Our results are seemingly similar to previous observations that *Tgfb2* and *Smad4* haploinsufficiency, expected to attenuate TGF-β signaling, increase aortic size and mortality of *Fbn1*[C1039G/+] mice (13, 20). However, in those studies, TGF-β signaling was paradoxically activated in aortic tissues in vivo. Although *Tgfbr2* exon2 deletion is not a model for kinase-mutant receptors in Loeys-Dietz syndrome, the similar medial degeneration in both situations suggests that either deficient or excess TGF-β signaling may disrupt SMC homeostasis. There are several examples of context-dependent roles of TGF-β in disease pathogenesis, such as either gain or loss of signaling in carcinoma cells promoting metastasis (49) or resulting in heterotaxy and congenital heart disease (50). In support of a protective role in arterial disease, TGF-β prevents aortic dilatation in various murine models of immunomediated vascular remodeling (51–54) and protects against immunologic injury of SMCs in experimental human systems of arteriosclerosis (55, 56). Specifically, diminished TGF-β responses in T cells of *Smad3*-deficient mice result in transmural inflammation of the aorta with aneurysm rupture, and the vascular phenotype is replicated in WT animals by adoptive transfer of *Smad3*^{–/–} bone marrow or CD4+ T cells (57).

While this work implies the need for caution when considering therapeutic use of nonspecific and potent TGF-β antagonists for aortic diseases, a number of considerations preclude immediate generalization of results made using models with a cell type–specific abrogation of TGF-β signaling to patients and mouse models with heterozygous loss-of-function mutations in genes encoding effectors of TGF-β signaling. Given that all aortic cell types in the latter group retain signaling potential, the requisites for paracrine overdrive of TGF-β signaling in response to excessive ligand production are maintained, including in the aortic media. In this light, it is notable that both mice and people with heterozygous mutations in the genes encoding fibrillin-1, TβRI, TβRII, Smad3, and TGF-β2 show enhanced Smad-dependent TGF-β signaling in the aortic media in association with postnatal aneurysm progression and dissection (8–20) and that phenotypic rescue in mice with agents such as losartan correlates with a reduction in TGF-β signaling in aortic SMCs (17). More recently, it was shown that loss-of-function mutations in the gene encoding the prototypical TGF-β repressor SKI, a perturbation predicted and observed to increase TGF-β signaling, cause aortic root aneurysm

in Shprintzen-Goldberg syndrome (58). Indeed, even in our work, the intense fibroproliferative response of the vessel wall and the increase in production of TGF-β ligands and output of TGF-β–responsive genes suggest that increased TGF-β signaling may contribute to disease manifestations. This extends to the aortic media, given the potential for incomplete efficiency of tamoxifen-induced recombination, as is notable in the mice with targeting of both *Tgfbr2* and *Fbn1*. The bottom line is that a productive balance in signaling among vascular cells, cell types, and compartments must be achieved for maximal therapeutic gain (59, 60).

In summary, our work addresses previously unanswered questions regarding the role of TGF-β in homeostasis of the postnatal arterial wall and underscores the context-dependent effects of TGF-β in aortic disease. In addition to overactivity and dysregulation of canonical versus noncanonical pathways, a loss of basal TGF-β signaling in smooth muscle also causes aortic dilatation and dissection. Caution is warranted in the use of potent TGF-β antagonists for aortic aneurysms that may oversuppress signaling across multiple mural cell types, particularly in children with growing aortas analogous to those of our postweanling animals. A mitigating strategy may be cotreatment with mTOR inhibitors that prevent vascular pathology arising from absent TGF-β responses.

Methods

Mice. *Tgfbr2*[f/f] mice (21) were obtained from H.L. Moses (Vanderbilt University, Nashville, Tennessee, USA). *Myh11-CreER*[T2] mice (22) and *Fbn1*[C1039G/+] mice (17) have been previously described. *Gt(ROSA)26Sor*[tm4(ACTB–tdTomato,–EGFP)Luo]/J (*mT/mG*) mice (23) were purchased from Jackson Laboratory. All strains had been backbred onto a C57BL/6 background for more than 8 generations. Male mice were euthanized at various ages for analysis (the bacterial artificial chromosome containing *Myh11-CreER*[T2] inserted on the Y chromosome and female mice do not express the construct).

Animal treatment. Cre-Lox recombination was induced by tamoxifen (Sigma-Aldrich) at 1 mg/d i.p. for 5 days starting at various ages versus vehicle (corn oil) alone. Certain animals were treated with BrdU (Sigma-Aldrich) at 1 mg s.c. every other day (q.o.d.) between 4 and 6 weeks of age, ML-7 (Enzo) at 73 μg/d s.c. constant infusion via implantable pump between 4 and 6 weeks of age, rapamycin (Calbiochem) at 2 mg/kg/d i.p. every day (q.d.) between 3 and 7 weeks of age with a final dose 24 hours before euthanasia, neutralizing antibody to IGF1 (clone 126002, R&D Systems) at 125 μg/d i.p. q.o.d. between 4 and 6 weeks of age with a final dose 6 hours before euthanasia, and neutralizing antibody to TGF-β1, -2, -3 (clone 1D11.16.8, BioXCell) at 250 μg/d i.p. q.o.d. between 4 and 6 or 4 and 8 weeks of age with a final dose 6 hours before euthanasia. The in vivo efficacy of the TGF-β blocking antibody has been previously validated (20).

Tissues. We analyzed the thoracic aorta since it was the primary site of overt pathology. Histology, immunohistochemistry, fluorescence microscopy, Western blotting, and quantitative RT-PCR were performed in the ascending aorta or an equal length segment of proximal descending aorta with similar results. The aortic root (from the aortic valve to the coronary arteries) was not dissected from the heart and was not included in the analyses.

Cells. Thoracic aortas were predigested for 5 minutes at 37°C in HBSS solution containing 1 mg/ml collagenase type A to promote sharp removal of the adventitia under a dissecting microscope. The denuded vessels were transferred into 2 to 3 ml HBSS solution containing 2 mg/ml collagenase type A and 0.5 mg/ml elastase and incubated at 37°C for 30 minutes while the digest was titrated with a pipette every 5 to 10 minutes. Digestion was stopped with growth medium, the mixture was centrifuged, and the cells were resuspended in Claycomb medium (Sigma-Aldrich) supplemented with 10% fetal bovine serum (Invitrogen) and cultured in T25 flasks in a

CO_2 incubator at 37°C. On reaching confluence, the cells were detached with trypsin, and GFP+ SMCs were sorted under sterile conditions using a FACSCalibur (BD Biosciences). The cells were serially expanded, and passages 3–6 were used for experiments. Signaling studies were performed after resting the SMCs in serum-free DMEM medium for 24 hours followed by treatment with TGF-β1, TGF-β2, TGF-β3, IGF1 (R&D Systems), and/or rapamycin (Calbiochem) at the indicated doses and times.

Vascular studies. Animals were anesthetized with isoflurane. B-mode ultrasound images of the ascending aorta in transverse and longitudinal planes were obtained using a Vevo 770 system (VisualSonics). For invasive hemodynamic analysis, the aorta was catheterized via the carotid artery using a 1.4-Fr Mikro-Tip pressure catheter (Millar Instruments), and blood pressure measurements were obtained using a PowerLab system (ADInstruments).

Histology. The vasculature was perfusion-fixed with 4% paraformaldehyde (PFA) via the left ventricle at 80 mmHg. For macroscopic examination, the aorta was exposed in situ and imaged with a dissecting microscope (Olympus). For histology, the aorta was excised and embedded in paraffin, and 5 μm-thick transverse sections were stained with H&E, elastin–Van Gieson (EVG), Masson's trichrome, and Sirius red using standard techniques. The histological sections were analyzed using ImageJ software (http://rsbweb.nih.gov/ij/) by outlining the arterial compartment perimeters to calculate mean area/thickness and by assessing staining intensity as pixel counts. Hematoxylin-stained nuclei within the media were counted in PFA-fixed, OCT-embedded sections and averaged from 3 high power fields.

Immunohistochemistry. Immunolabeling of 5 μm-thick, paraffin-embedded aorta sections was performed with primary antibodies to BrdU (Abcam), CD45 (Abnova), TER119 (R&D Systems), SMA (Sigma-Aldrich), p-S6K, p-Smad2 (ser465/467), p-MLC (all from Cell Signaling), or isotype-matched, irrelevant IgG. Binding of secondary antibody (Jackson ImmunoResearch) was detected with vectastain ABC reagent and AEC peroxidase substrate kits (Vector Laboratories), counterstained with hematoxylin, and imaged using an Axioskop2 Plus microscope (Carl Zeiss MicroImaging). Additionally, PFA-fixed, OCT-embedded tissue sections were incubated with CD45 antibody (BD Biosciences). Cultured cells were fixed with 4% PFA, permeabilized with 0.1% Triton X-100, and denatured with 2 M HCL for 10 minutes prior to BrdU antibody labeling.

Fluorescence microscopy. For studies of reporter mice, aortas were perfused with cold 4% PFA in 0.1 M PBS (Sigma-Aldrich), fixed overnight in 4% PFA at 4°C, cryoprotected in 15% sucrose for 6 to 8 hours at 4°C, and embedded in OCT (Tissue-Tek), and 5-μm–thick sections were obtained using a Leica cryostat. For immunofluorescence analysis, 5-μm–thick, paraffin-embedded aorta sections were labeled with antibodies to Ki-67 (Abcam), p-MLC, p-Smad2 (ser465/467), p-ERK1/2 (Thr202/Tyr204) (all from Cell Signaling), or isotype-matched, irrelevant IgG. Detection of primary antibodies was visualized with Alexa Fluor 594–conjugated goat anti-rabbit IgG (Invitrogen). FITC-conjugated anti-SMA (Sigma-Aldrich) was added for double staining of SMCs. Sections were mounted with ProLong Gold antifade reagent with DAPI (Invitrogen) and imaged using an Axiovert 200M microscopy system with AxioVision 4.6 software (Carl Zeiss MicroImaging). Alternatively, SMCs cultured on sterile glass coverslips were fixed and permeabilized, as for immunohistochemistry, prior to incubation with antibodies.

Immunoblotting. Protein was extracted from aortas and SMCs using RIPA lysis buffer containing a protease inhibitor cocktail (Thermo Scientific) with PhosSTOP (Roche) and boiled in SDS sample buffer for 6 minutes. Equal amounts of protein per sample were separated by SDS-PAGE, transferred electrophoretically to a nitrocellulose membrane (Bio-Rad Laboratories), and blotted with antibodies against TβRII extracellular domain (R&D Systems), p-Smad2 (ser465/467, clone 138D4), Smad2 (clone L16D3), p-p38 (Thr180/Tyr182), p38, p-ERK1/2, p-MLC, MLC,

p-myosin phosphatase target subunit-1 (p-MYPT1), p-AKT (Thr308), p-S6K, S6K, p-S6, S6 (all from Cell Signaling), ERK1/2 (Santa Cruz Biotechnology Inc.), SMA, SM22, SMMHC (all from Abcam), and β-actin (Sigma-Aldrich), followed by horseradish peroxidase–conjugated secondary antibodies (Jackson ImmunoResearch). A different p-Smad2 antibody (ser465/467; Millipore) was used in certain experiments after a batch change in the initial reagent. Bound antibody was detected with Western Lightning Plus-ECL (PerkinElmer).

RT-PCR. Crushed aortic tissue or scraped cells were immersed in RLT lysis buffer (QIAGEN) and vigorously vortexed, and total RNA was isolated using RNeasy Mini Kits and DNA digestion kits (QIAGEN) according to the manufacturer's protocol. RT with random hexamer and oligo-dT primers was performed according to the Multiscribe RT system protocol (Applied Biosystems). PCR was performed using cDNA, PCR Redmix (Sigma-Aldrich), and primers specific for *Tgfbr2* exon2 (forward 5′-TTAA-CATGATGTCATGGCCAGCG-3′ and reverse 5′-AGACTTCATGCG-GCTTCTCACAGA-3′); the solution was separated by 1.5% agarose gel using 18S RNA as a control. Real-time quantitative RT-PCR reactions were prepared with TaqMan PCR Master Mix and predeveloped assay reagents from Applied Biosystems. Samples were analyzed on an iCycler (Bio-Rad Laboratories). RNA samples processed without the RT enzyme were used as negative controls. The expression level of each transcript was normalized to that of Hprt1 as $\log_2$ (reference gene – gene of interest quantification cycle). We confirmed stable expression of Hprt1 under our experimental conditions with significant correlation ($r = 0.9529$–0.9912, $P < 0.0001$, Pearson test) to 2 other reference transcripts of Gapdh and Actb in a subset of in vitro ($n = 18$) and in vivo ($n = 18$) samples.

Laser capture microdissection. Aortas were cut into 5-μm sections and placed on charged slides prior to fixation in 70% ethanol. The slides were stained with H&E, rinsed in an ethanol gradient, and dehydrated in a xylene mixture. The adventitia and media were sequentially procured using a Pixcell laser capture microscope (Arcturus Engineering) and transferred to CapSure films (Arcturus Engineering); RNA was isolated for quantitative RT-PCR.

Microarray analysis. Ascending aortas were harvested from 6-week-old *Myh11-CreER^T2.Tgfbr2^f/f* and *Fbn1^C1039G/+.Myh11-CreER^T2.Tgfbr2^f/f* littermates treated with vehicle or tamoxifen at 4 weeks of age ($n = 3$ in each of the 4 groups). Preparation of sscDNA and hybridization to the mouse GeneChip set (1.0 ST Array) were performed according to the manufacturer's protocol (Affymetrix). The stained chips were read and analyzed with GeneChip Scanner 3000 (Affymetrix). Expression intensities were quantified and compared using Partek Genomics Suite v6.4 (Partek Inc.) with robust multi-array average for normalization and fold-change calculations. Comparisons of $\log_2$-transformed data were by unpaired *t* test after filtering for false discovery rate to correct for multiple comparisons. For the purposes of this study, gene expression differences that differed by more than 2-fold relative to comparison groups with *P* values of less than 0.05 were considered significant. The primary microarray data have been deposited in the Gene Expression Omnibus (GSE36778).

Flow cytometry. GFP+ SMCs were labeled with biotinylated antibody to the extracellular domain of TβRII (R&D Systems) and APC-conjugated anti-biotin antibody or isotype-matched, irrelevant IgG. Analysis was performed using a FACSCalibur and FlowJo 7.0 software.

Collagen gels. GFP+ SMCs were suspended at 2.5×10^5 cells/ml in type I collagen at 2.5 mg/ml (BD Biosciences) with 10 μl/ml 1N NaOH. The mixture was poured into 24-well tissue culture plates (1 ml/2 cm² well) that were precoated with 1% gelatin and allowed to polymerize in a 5% CO_2 incubator at 37°C for 30 minutes; 1 ml of growth medium was added. Gel contraction was assessed at 72 hours by scanning the plates and determining surface area using NIH ImageJ.

Statistics. Data represent mean ± SEM. Unpaired *t* test was used for comparisons between 2 groups, 1-way ANOVA was used for comparisons between more than 2 groups followed by the Newman-Keuls Multiple Comparison test, logrank test was used to compare survival curves, χ^2 test was used to analyze contingency tables, and Pearson test was used to determine correlations. *P* values were 2-tailed and values of less than 0.05 were considered statistically significant. Data were analyzed using Prism 4.0 software (GraphPad).

Study approval. Animal studies were approved by the Institutional Animal Care and Use Committee of Yale University.

Address correspondence to: George Tellides, 10 Amistad Street 337B, P.O. Box 208089, New Haven, Connecticut 06520, USA. Phone: 203.737.2298; Fax: 203.737.6386; E-mail: george.tellides@yale.edu. Or to: Wei Li, Department of Vascular Surgery, Peking University People's Hospital, No. 11 Xizhimen South Street, Xicheng District, Beijing, 100044, People's Republic of China. Phone: 86.10.88324752; E-mail: weili@bjmu.edu.cn.

1. Pardali E, Goumans MJ, ten Dijke P. Signaling by members of the TGF-β family in vascular morphogenesis and disease. *Trends Cell Biol.* 2010;20(9):556–567.
2. Oshima M, Oshima H, Taketo MM. TGF-β receptor type II deficiency results in defects of yolk sac hematopoiesis and vasculogenesis. *Dev Biol.* 1996;179(1):297–302.
3. Larsson J, et al. Abnormal angiogenesis but intact hematopoietic potential in TGF-β type I receptor-deficient mice. *EMBO J.* 2001;20(7):1663–1673.
4. Carvalho RL, et al. Compensatory signalling induced in the yolk sac vasculature by deletion of TGFβ receptors in mice. *J Cell Sci.* 2007;120(pt 24):4269–4277.
5. Wurdak H, et al. Inactivation of TGFβ signaling in neural crest stem cells leads to multiple defects reminiscent of DiGeorge syndrome. *Genes Dev.* 2005;19(5):530–535.
6. Wang J, Nagy A, Larsson J, Dudas M, Sucov HM, Kaartinen V. Defective ALK5 signaling in the neural crest leads to increased postmigratory neural crest cell apoptosis and severe outflow tract defects. *BMC Dev Biol.* 2006;6:51.
7. Choudhary B, Zhou J, Li P, Thomas S, Kaartinen V, Sucov HM. Absence of TGFβ signaling in embryonic vascular smooth muscle leads to reduced lysyl oxidase expression, impaired elastogenesis, and aneurysm. *Genesis.* 2009;47(2):115–121.
8. Loeys BL, et al. A syndrome of altered cardiovascular, craniofacial, neurocognitive and skeletal development caused by mutations in TGFBR1 or TGFBR2. *Nat Genet.* 2005;37(3):275–281.
9. Mizuguchi T, et al. Heterozygous TGFBR2 mutations in Marfan syndrome. *Nat Genet.* 2004;36(8):855–860.
10. Inamoto S, et al. TGFBR2 mutations alter smooth muscle cell phenotype and predispose to thoracic aortic aneurysms and dissections. *Cardiovasc Res.* 2010;88(3):520–529.
11. Maleszewski JJ, Miller DV, Lu J, Dietz HC, Halushka MK. Histopathologic findings in ascending aortas from individuals with Loeys-Dietz syndrome (LDS). *Am J Surg Pathol.* 2009;33(2):194–201.
12. Boileau C, et al. TGFB2 mutations cause familial thoracic aortic aneurysms and dissections associated with mild systemic features of Marfan syndrome. *Nat Genet.* 2012;44(8):916–921.
13. Lindsay ME, et al. Loss-of-function mutations in TGFB2 cause a syndromic presentation of thoracic aortic aneurysm. *Nat Genet.* 2012;44(8):922–927.
14. Gomez D, et al. Syndromic and non-syndromic aneurysms of the human ascending aorta share activation of the Smad2 pathway. *J Pathol.* 2009;218(1):131–142.
15. Renard M, et al. Novel MYH11 and ACTA2 mutations reveal a role for enhanced TGFβ signaling in FTAAD. *Int J Cardiol.* 2013;165(2):314–321.
16. Neptune ER, et al. Dysregulation of TGF-β activation contributes to pathogenesis in Marfan syndrome. *Nat Genet.* 2003;33(3):407–411.
17. Habashi JP, et al. Losartan, an AT1 antagonist, prevents aortic aneurysm in a mouse model of Marfan syndrome. *Science.* 2006;312(5770):117–121.
18. Carta L, et al. p38 MAPK is an early determinant of promiscuous Smad2/3 signaling in the aortas of fibrillin-1 (Fbn1)-null mice. *J Biol Chem.* 2009;284(9):5630–5636.
19. Brooke BS, Habashi JP, Judge DP, Patel N, Loeys B, Dietz HC 3rd. Angiotensin II blockade and aortic-root dilation in Marfan's syndrome. *N Engl J Med.* 2008;358(26):2787–2795.
20. Holm TM, et al. Noncanonical TGFβ signaling contributes to aortic aneurysm progression in Marfan syndrome mice. *Science.* 2011;332(6027):358–361.
21. Bhowmick NA, et al. TGF-β signaling in fibroblasts modulates the oncogenic potential of adjacent epithelia. *Science.* 2004;303(5659):848–851.
22. Wirth A, et al. G12-G13-LARG-mediated signaling in vascular smooth muscle is required for salt-induced hypertension. *Nat Med.* 2008;14(1):64–68.
23. Muzumdar MD, Tasic B, Miyamichi K, Li L, Luo L. A global double-fluorescent Cre reporter mouse. *Genesis.* 2007;45(9):593–605.
24. Hautmann MB, Madsen CS, Owens GK. A transforming growth factor β (TGFβ) control element drives TGFβ-induced stimulation of smooth muscle α-actin gene expression in concert with two CArG elements. *J Biol Chem.* 1997;272(16):10948–10956.
25. Milewicz DM, et al. Genetic basis of thoracic aortic aneurysms and dissections: focus on smooth muscle cell contractile dysfunction. *Annu Rev Genomics Hum Genet.* 2008;9:283–302.
26. Birukova AA, Adyshev D, Gorshkov B, Birukov KG, Verin AD. ALK5 and Smad4 are involved in TGF-β1-induced pulmonary endothelial permeability. *FEBS Lett.* 2005;579(18):4031–4037.
27. Kita T, et al. Role of TGF-β in proliferative vitreoretinal diseases and ROCK as a therapeutic target. *Proc Natl Acad Sci U S A.* 2008;105(45):17504–17509.
28. Wang L, et al. Mutations in myosin light chain kinase cause familial aortic dissections. *Am J Hum Genet.* 2010;87(5):701–707.
29. Kuang SQ, et al. Rare, nonsynonymous variant in the smooth muscle-specific isoform of myosin heavy chain, MYH11, R247C, alters force generation in the aorta phenotype of smooth muscle cells. *Circ Res.* 2012;110(11):1411–1422.
30. Papke CL, et al. Smooth muscle hyperplasia due to loss of smooth muscle α-actin is driven by activation of focal adhesion kinase, altered p53 localization increased levels of platelet-derived growth factor receptor-β. *Hum Mol Genet.* 2013;22(15):3123–3137.
31. Tang PC, et al. Hyperplastic cellular remodeling of the media in ascending thoracic aortic aneurysms. *Circulation.* 2005;112(8):1098–1105.
32. Milewicz DM, Kwartler CS, Papke CL, Regalado ES, Cao J, Reid AJ. Genetic variants promoting smooth muscle cell proliferation can result in diffuse and diverse vascular diseases: evidence for a hyperplastic vasculomyopathy. *Genet Med.* 2010; 12(4):196–203.
33. Pannu H, et al. MYH11 mutations result in a distinct vascular pathology driven by insulin-like growth factor 1 angiotensin II. *Hum Mol Genet.* 2007;16(20):2453–2462.
34. Cao J, et al. Thoracic aortic disease in tuberous sclerosis complex: molecular pathogenesis and potential therapies in Tsc2⁺/⁻ mice. Thoracic aortic disease in tuberous sclerosis complex: molecular pathogenesis and potential therapies in Tsc2⁺/⁻ mice. *Hum Mol Genet.* 2010;19(10):1908–1920.
35. Li W, et al. Rapamycin inhibits smooth muscle cell proliferation and obstructive arteriopathy attributable to elastin deficiency. *Arterioscler Thromb Vasc Biol.* 2013;33(5):1028–1035.
36. Yamashita M, Fatyol K, Jin C, Wang X, Liu Z, Zhang YE. TRAF6 mediates Smad-independent activation of JNK p38 by TGF-β. *Mol Cell.* 2008;31(6):918–924.
37. Simeone DM, et al. Smad4 mediates activation of mitogen-activated protein kinases by TGF-β in pancreatic acinar cells. *Am J Physiol Cell Physiol.* 2001;281(1):C311–C319.
38. Lee MK, et al. TGF-β activates Erk MAP kinase signalling through direct phosphorylation of ShcA. *EMBO J.* 2007;26(17):3957–3967.
39. Iwata J, Hacia JG, Suzuki A, Sanchez-Lara PA, Urata M, Chai Y. Modulation of noncanonical TGF-β signaling prevents cleft palate in Tgfbr2 mutant mice. *J Clin Invest.* 2012;122(3):873–885.
40. Martin KA, et al. The mTOR/p70 S6K1 pathway regulates vascular smooth muscle cell differentiation. *Am J Physiol Cell Physiol.* 2004;286(3):C507–C517.
41. Lawrence DM, Singh RS, Franklin DP, Carey DJ, Elmore JR. Rapamycin suppresses experimental aortic aneurysm growth. *J Vasc Surg.* 2004;40(2):334–338.
42. Moran CS, et al. Everolimus limits aortic aneurysm in the apolipoprotein E-deficient mouse by downregulating C-C chemokine receptor 2 positive monocytes. *Arterioscler Thromb Vasc Biol.* 2013;33(4):814–821.
43. Lindsay ME, Dietz HC. Lessons on the pathogenesis of aneurysm from heritable conditions. *Nature.* 2011;473(7347):308–316.
44. Forte A, Della Corte A, De Feo M, Cerasuolo F, Cipollaro M. Role of myofibroblasts in vascular remodelling: focus on restenosis and aneurysm. *Cardiovasc Res.* 2010;88(3):395–405.
45. Tang PC, et al. MyD88-dependent, superoxide-initiated inflammation is necessary for flow-mediated inward remodeling of conduit arteries. *J Exp Med.* 2008;205(13):3159–3171.
46. Zhou J, et al. CXCR3-dependent accumulation activation of perivascular macrophages is necessary for homeostatic arterial remodeling to hemodynamic stresses. *J Exp Med.* 2010;207(9):1951–1966.
47. Michel JB, Thaunat O, Houard X, Meilhac O, Caligiuri G, Nicoletti A. Topological determinants and consequences of advential responses

to arterial wall injury. *Arterioscler Thromb Vasc Biol.* 2007;27(6):1259–1268.

48. Majesky MW, Dong XR, Hoglund V, Mahoney WM Jr, Daum G. The adventitia: a dynamic interface containing resident progenitor cells. *Arterioscler Thromb Vasc Biol.* 2011;31(7):1530–1539.

49. Bierie B, Moses HL. Gain or loss of TGFβ signaling in mammary carcinoma cells can promote metastasis. *Cell Cycle.* 2009;8(20):3319–3327.

50. Fakhro KA, et al. Rare copy number variations in congenital heart disease patients identify unique genes in left-right patterning. *Proc Natl Acad Sci U S A.* 2011;108(7):2915–2920.

51. Dai J, et al. Overexpression of transforming growth factor-β1 stabilizes already-formed aortic aneurysms: a first approach to induction of functional healing by endovascular gene therapy. *Circulation.* 2005;112(7):1008–1015.

52. Frutkin AD, et al. TGF-β1 limits plaque growth, stabilizes plaque structure, prevents aortic dilation in apolipoprotein E-null mice. *Arterioscler Thromb Vasc Biol.* 2009;29(9):1251–1257.

53. Wang Y, et al. TGF-β activity protects against inflammatory aortic aneurysm progression and complications in angiotensin II-infused mice. *J Clin Invest.* 2010;120(2):422–432.

54. Dai J, et al. Long term stabilization of expanding aortic aneurysms by a short course of cyclosporine A through transforming growth factor-β induction. *PLoS One.* 2011;6(12):e28903.

55. Lebastchi AH, et al. Activation of human vascular cells decreases their expression of transforming growth factor-β. *Atherosclerosis.* 2011;219(2):417–424.

56. Lebastchi AH, et al. Transforming growth factor β expression by human vascular cells inhibits interferon γ production and arterial media injury by alloreactive memory T cells. *Am J Transplant.* 2011;11(11):2332–2341.

57. Ye P, et al. GM-CSF contributes to aortic aneurysms resulting from SMAD3 deficiency. *J Clin Invest.* 2013;123(5):2317–2331.

58. Doyle AJ, et al. Mutations in the TGF-β repressor SKI cause Shprintzen-Goldberg syndrome with aortic aneurysm. *Nat Genet.* 2012;44(11):1249–1254.

59. Jones JA, Spinale FG, Ikonomidis JS. Transforming growth factor-β signaling in thoracic aortic aneurysm development: a paradox in pathogenesis. *J Vasc Res.* 2009;46(2):119–37.

60. Dietz HC. TGF-β in the pathogenesis and prevention of disease: a matter of aneurysmic proportions. *J Clin Invest.* 2010;120(2):403–407.